The Astrophysical Journal, 832:59 (7pp), 2016 November 20 doi:10.3847/0004-637X/832/1/59

CONSTRAINING THE SOLAR CORONAL MAGNETIC FIELD STRENGTH USING SPLIT-BAND TYPE II RADIO BURST OBSERVATIONS

P. Kishore[1], R. Ramesh[1], K. Hariharan[1], C. Kathiravan[1], and N. Gopalswamy[2]
[1] Indian Institute of Astrophysics, 2nd Block, Koramangala, Bangalore—560034, India; kishore@iiap.res.in
[2] Code 671, Solar Physics Laboratory, NASA/GSFC, Greenbelt, MD 20771 USA
Received 2016 April 13; revised 2016 September 14; accepted 2016 September 16; published 2016 November 17

ABSTRACT

We report on low-frequency radio (85–35 MHz) spectral observations of four different type II radio bursts, which exhibited fundamental-harmonic emission and split-band structure. Each of the bursts was found to be closely associated with a whitelight coronal mass ejection (CME) close to the Sun. We estimated the coronal magnetic field strength from the split-band characteristics of the bursts, by assuming a model for the coronal electron density distribution. The choice of the model was constrained, based on the following criteria: (1) when the radio burst is observed simultaneously in the upper and lower bands of the fundamental component, the location of the plasma level corresponding to the frequency of the burst in the lower band should be consistent with the deprojected location of the leading edge (LE) of the associated CME; (2) the drift speed of the type II bursts derived from such a model should agree closely with the deprojected speed of the LE of the corresponding CMEs. With the above conditions, we find that: (1) the estimated field strengths are unique to each type II burst, and (2) the radial variation of the field strength in the different events indicate a pattern. It is steepest for the case where the heliocentric distance range over which the associated burst is observed is closest to the Sun, and vice versa.

Key words: solar–terrestrial relations – Sun: activity – Sun: corona – Sun: coronal mass ejections (CMEs) – Sun: magnetic fields – Sun: radio radiation

1. INTRODUCTION

Type II radio bursts from the Sun are caused by Langmuir waves generated by nonthermal electrons in magnetohydrodynamic (MHD) shocks propagating outward in the solar atmosphere. The characteristics and description of the solar type II bursts can be found in the review by Nelson & Melrose (1985). The bursts are observed as narrow-band emission features drifting from higher to lower frequencies in spectral observations. They occur frequently as two relatively slow drifting emission bands (fundamental (F) and harmonic (H)) with a frequency ratio of ≈1:2. The frequency drift (typically ∼0.1 MHz s^{-1}, see Mann et al. 1996; Gopalswamy et al. 2009) results from the decrease of the coronal electron density (N_e) and hence the plasma frequency, with increasing distance (r) from the Sun. The observed drift rate can be converted into the speed of the associated MHD shock if the $N_e(r)$ is known. At times, type II bursts exhibit split-band structure: either or both the F and H components of the burst are split into two subbands (the upper band U and the lower band L) with a separation in frequency, which is usually small compared to the frequency separation between the F and H components themselves. The L and U bands in a split-band type II burst are considered to be due to emission generated ahead of and behind the associated MHD shock front, i.e., at the upstream and downstream regions or the pre-shock and post-shock regions or the "undisturbed" and "disturbed" corona, respectively (Tidman et al. 1966; Vršnak et al. 2001; Hariharan et al. 2014).

It was first shown by Smerd et al. (1974, 1975) that type II solar radio bursts that exhibit split-band structure can be used to determine the magnetic field strength ($B(r)$) along the paths of the propagating MHD shocks. Note that magnetic field strength is routinely measured only in the photosphere at present. The magnetic field strength of the "undisturbed" corona is obtained from such measurements using extrapolation techniques (Schatten et al. 1969; Schrijver & Derosa 2003). Although estimates of coronal magnetic field strength ($B(r)$) from observations in infrared, microwave, and EUV wavelength bands (Lin et al. 2000; Lee 2007; West et al. 2011) are possible, they are limited mostly to the "inner" corona ($r \lesssim 1.2\ R_\odot$). But phenomena like the acceleration of energetic particles by coronal mass ejection (CME) driven shocks, acceleration of fast solar wind, etc., occur typically in the "middle" corona, i.e., $1.2\ R_\odot \lesssim r \lesssim 3.0\ R_\odot$ (Gopalswamy et al. 2012b; Mancuso & Garzelli 2013). There are estimates of $B(r)$ in the above heliocentric distance range from the spectral observations of split-band type II solar radio bursts (Smerd et al. 1974, 1975; Vršnak et al. 2002; Cho et al. 2007; Zimovets et al. 2012; Mancuso & Garzelli 2013; Hariharan et al. 2014, 2015; Vasant et al. 2014). But the locations of the bursts at different frequencies, and hence the B at the corresponding values of r, were derived without referring to the deprojected height-time details of the associated shock driver. Considering that there is close spatio-temporal association between the type II bursts and the CMEs (Stewart et al. 1974a, 1974b; Gopalswamy & Kundu 1992; Mancuso & Raymond 2004; Gopalswamy et al. 2005, 2009; Lin et al. 2006; Cho et al. 2008, 2013; Liu et al. 2009; Ramesh et al. 2010, 2012; Ma et al. 2011; Hariharan et al. 2014, 2015; Kouloumvakos et al. 2014), we have attempted to derive $B(r)$ by constraining the choice of $N_e(r)$ and consequently the locations of the bursts based on the observed parameters of the type II bursts and the accompanying CMEs together. There is considerable evidence for this method, because the starting frequency of the type II bursts has a power-law relationship with the leading edge (LE) of the associated CMEs, as was shown by Gopalswamy et al. (2013). Note that the most important requirement for the estimation of $B(r)$ from a type II burst, which exhibits a band-splitting phenomenon is the identification of the appropriate $N_e(r)$ model, which can satisfactorily explain the observed

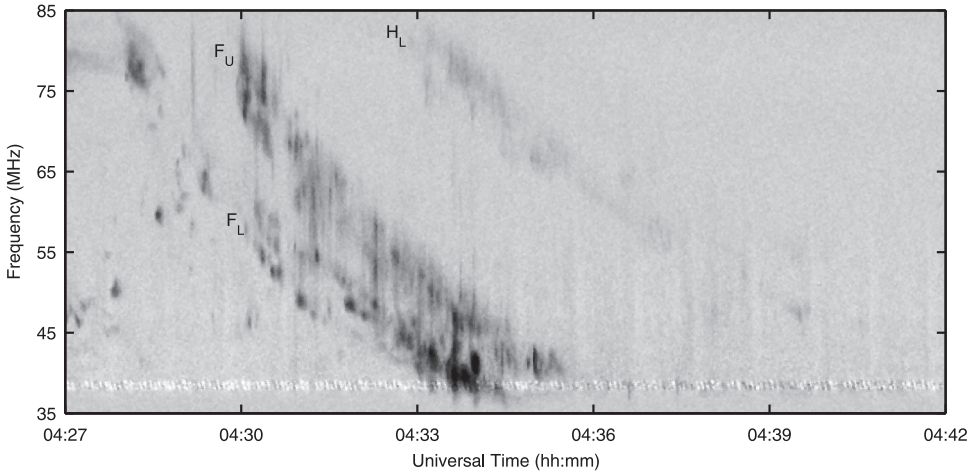

Figure 1. Dynamic spectrum (85–35 MHz) of the type II radio burst from the solar corona obtained with the GLOSS on 2013 November 8 during 04:27–04:42 UT. The *F* and *H* components of the type II burst with band splitting (in the *F* component) are clearly noticeable. The labels F_L and F_U represent the lower and upper bands in the *F* component of the type II burst. The white horizontal line close to 35 MHz is due to local radio frequency interference (RFI).

characteristics of the burst since $B(r)$ is more sensitive to it (see for example Cho et al. 2007).

2. OBSERVATIONS

The radio spectral data were obtained during the period 2013 October–2014 February with the Gauribidanur LOw frequency Solar Spectrograph (GLOSS) in the Gauribidanur observatory[3], located about 100 km north of Bangalore in India (Ramesh 2011). It is a total power instrument operating in the frequency range 85–35 MHz. The primary receiving element used is a log-periodic dipole antenna (LPDA, Ebenezer et al. 2001, 2007; Kishore et al. 2014). The primary receiving element used is a log-periodic dipole antenna (LPDA, Carrel 1961). Eight such LPDAs, arranged in the north–south direction with a spacing of ≈5 m between the adjacent antennae, have been combined in a branched feeder system to generate a single output (see for example Ramesh et al. 1998). The half-power width of the response pattern ("beam") of the GLOSS at a typical frequency such as 80 MHz is ≈90° × 6° (R.A. × decl.). The integration time is ≈100 ms and the observing bandwidth is ≈300 kHz at each frequency. The width of the beam of the GLOSS in R.A. (i.e., hour angle) is nearly independent of frequency. The beam can be steered in declination by including switchable cable delay lines in the aforementioned branched feeder system. The minimum detectable flux density (1σ level) with the GLOSS is ≈3000 Jy ($1\ \mathrm{Jy} = 10^{-26}\ \mathrm{Wm^{-2}\ Hz^{-1}}$). We specifically chose the above period for the present work, since the Sun was closer to the Galactic Center (GC) in both R.A. and decl., and it facilitated the calibration of the antennae in the GLOSS array (Ramesh et al. 2013; Kishore et al. 2015). Even here, we have considered only those type II bursts, which showed both split-band and *F–H* structure, and there was simultaneous availability of CME observations in white light near the Sun ($<2\ R_\odot$). We used images obtained with the COR1 coronagraph of the Sun–Earth Connection Coronal and Heliospheric Investigation (Howard et al. 2008) on board the *Solar TErrestrial RElations Observatory* (*STEREO*), and the Large Angle and Spectrometric Coronagraph (Brueckner et al. 1995) on board the *Solar and Heliospheric Observatory* (*SOHO*) for information on the associated CMEs. For flare information, we used soft X-ray data obtained with the *Geostationary Operational Environmental Satellite* (*GOES*).

Figure 1 shows the dynamic spectrum of a typical split-band type II burst observed with the GLOSS on 2013 November 8 during the interval 04:27–04:42 UT in the frequency range 85–35 MHz. The splitting of the *F* component into lower (L) and upper (U) bands, i.e., F_L and F_U, can be clearly seen. In the *H* component, only the H_L band could be seen. The H_U band is close to the detection limit of GLOSS and hence, unnoticeable in the dynamic spectrum (see Figure 2). The onset times of the F_L and F_U bands at a typical frequency such as 80 MHz are ≈04:28 UT and ≈04:30 UT, respectively. They are last observed at ≈40 MHz at ≈04:34 UT and ≈04:35 UT, respectively. The duration of the F_L, F_U, H_L and H_U bands estimated from their temporal profile at 80 MHz are t_{fl}: $t_{fu} \approx 1{:}2$ and t_{hl}: $t_{hu} \approx 1{:}1.7$ (see Figure 2). The frequency ratio of the F_L and H_L bands estimated from the respective maximum amplitudes (f_l and h_l) in the spectral profile at ≈04:33 UT are f_l: $h_l \approx 1{:}2$ (see Figure 3). The ratio of the corresponding instantaneous bandwidths F_L: H_L is ≈1:1. These values are consistent with those reported in the literature for split-band type II radio bursts (see for example Hariharan et al. 2014). An inspection of the e-CALLISTO solar radio spectrometer (Monstein et al. 2007; Benz et al. 2009) observations at the Gauribidanur Observatory in the frequency range 45–440 MHz revealed that the above type II burst was limited to frequencies $\lesssim$150 MHz. The *STEREO-B* COR1 coronagraph observed a CME in close temporal association with the burst. The first appearance of the CME in the field of view (FOV) of *STEREO-B* COR1 was at ≈04:45 UT. The angular width of the CME was ≈24°, and its LE was at ≈1.8 $R_\odot$. There was also a X1.1 class *GOES* soft X-ray flare from the NOAA active region AR11890[4] located at S13E13. The above active region had 15 spots and $\beta - \delta$ configuration. Its total area was ≈480 millionths of the solar disk.[5] Note that STEREO-B was behind the Earth at ≈E144 in the above epoch.[6] This implies that AR11890 was at ≈W131 (i.e., ≈41° behind the limb) for the

[3] http://www.iiap.res.in/centers/radio

[4] ftp://ftp.swpc.noaa.gov/pub/warehouse

[5] http://www.lmsal.com/solarsoft/latest_events/

[6] http://stereo-ssc.nascom.nasa.gov/cgi-bin/make_where_gif

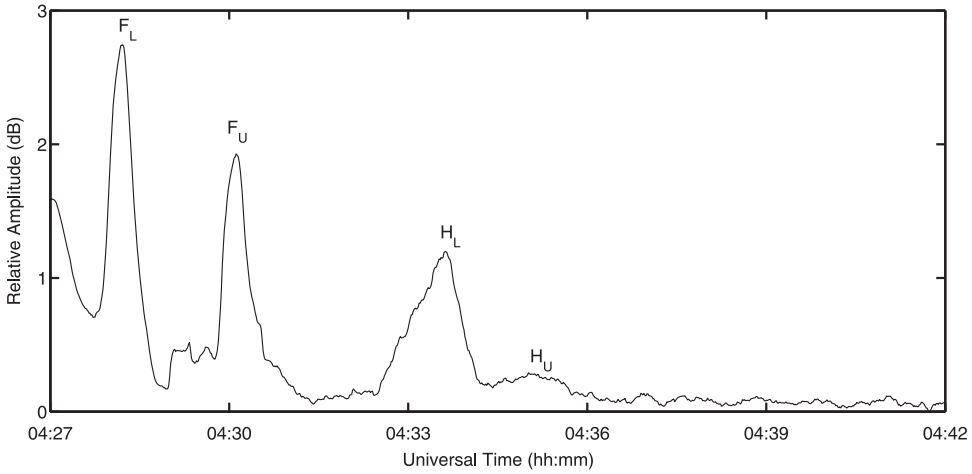

Figure 2. Temporal profile of the type II burst in Figure 1 at 80 MHz showing emission corresponding to the F_L, F_U, H_L, and H_U bands.

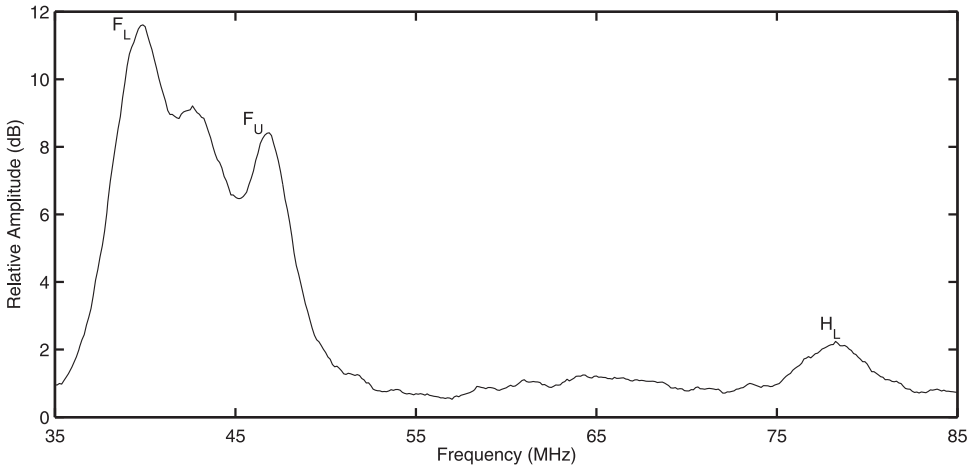

Figure 3. Spectral profile of the type II burst in Figure 1 at ≈04:33 UT. The emission corresponding to the F_L, F_U, and H_L bands can be seen. The H_U was not observable during the above time (see Figure 1).

STEREO-B view. Assuming that the projection effects vary as $1/\cos(\phi)$, where ϕ is the angle from the plane of the sky (POS), we calculated the deprojected location of the CME LE (r_{CME}) at ≈04:45 UT to be ≈2.33 $R_\odot$. The corresponding location at ≈04:50 UT is ≈2.64 $R_\odot$. The speed of the CME LE (v_{CME}) calculated from the above values is ≈719 km s^{-1}. Although the above values of r_{CME} and v_{CME} correspond to the LE of the CME, in the present case they can also be considered to be nearly the same for the flank of the CME, since the angular width of the CME is small (≈24°) in the STEREO-B COR1 FOV. Note that the type II burst in Figure 1 was observed before the CME appeared in the *STEREO-B* COR1 FOV at ≈04:45 UT. This implies that the angular width of the CME could have been $\lesssim$24° during the type II burst period. So the above assumption regarding r_{CME} and v_{CME} is reasonable. The details related to the type II bursts, flares, CMEs, and the coronal electron density distribution reported in the present work are listed in Table 1.

3. RESULTS AND ANALYSIS

An inspection of Figure 1 indicates that the earliest time at which the type II burst can be noticed simultaneously in both the F_L and F_U bands is ≈04:30 UT. The burst was present at frequency (f_s) ≈ 60 MHz in the F_L band at the above epoch. An extrapolation of the h–t locations of the associated CME mentioned in Section 2 indicates that $r_{CME} \approx 1.65\ R_\odot$ at ≈04:30 UT. We adopted different coronal electron density models (Baumbach 1937; Allen 1947; Newkirk 1961; Saito et al. 1977; Vršnak et al. 2004) in order to identify the particular model(s) that satisfies the following criteria for the type II bursts caused by CME-driven shock: (1) the location of the plasma level (r_{radio}) corresponding to f_s should be consistent with r_{CME} at the same time as the occurrence of f_s; (2) the drift speed (v_{typeII}) of the type II bursts based on such a model for $N_e(r)$ should agree closely with the v_{CME} of the corresponding CMEs. Note that all the above density models are applicable in the "middle" corona, where the density falls off typically as r^{-6} (Leblanc et al. 1998). After various trials, finally we found that both the aforementioned criteria were satisfied for all the four type II bursts and the associated CMEs by adopting the Saito model with suitable density enhancement factor (D) for each burst. For example, in the case of the type II burst of 2013 November 8 (Figure 1), we find that 6× Saito model gives the best results. The estimated $r_{typeII} \approx 1.61\ R_\odot$ corresponding to f_s = 68 MHz at ≈04:40 UT (see columns 3, 4 and 11 in Table 1) agrees closely with the $r_{CME} \approx 1.67\ R_\odot$ at the above epoch. The estimated $v_{typeII} \approx 843$ km s^{-1}, obtained after satisfactorily addressing the first criteria mentioned above, is reasonably close to $v_{CME} \approx 719$ km s^{-1}. The drift rate of the

Table 1
Details Related to Type II Bursts, Flares, CMEs, $N_e(r)$, and $B(r)$

S.No.	Date	Type II Burst		X-ray Flare Class/ Location	Spacecraft[b]/ Location	CME LE[c]		CME Width[c] (deg.)	$N_e(r)$ Model[f]	r_{typeII} Range ($R_\odot$)	v_{typeII} (km s^{-1})	$B(r)$ Range (G)
		Freq. Range[a] (MHz)	Onset Time (UT)			Proj./ de-proj. r_{CME}[d] ($R_\odot$)	Proj./ de-proj. v_{CME} (km s^{-1})					
1	2013 Oct 08	68–51	04:50	B6.9/ S13E63	S-B/E140	1.58/1.67	411/435	29	6S	1.61–1.77	555	1.73–1.32
									2G	1.63–1.76	431	1.34–01.02
2	2013 Nov 08	60–37	04:30	X1.1/ S13E13	S-B/E144	1.25/1.65	549/719	24	6S	1.67–1.97	843	1.80-1.30
									2G	1.68–1.91	635	1.35-0.97
3	2013 Nov 19	61–36	10:29	X1.0/ S13W69	S-A/W149	1.96/2.00	878/894	40[e]	17S	2.00–2.40	711	1.50–1.11
									8G	2.01–2.30	503	1.00–0.80
4	2014 Feb 10	43-38	05:16	C3.0/ S12E29	S-B/E158	1.56/2.02	696/900	14	9S	2.01–2.12	847	1.17–1.04
									4G	2.01–2.09	620	0.86–0.76

Notes.
[a] Corresponds to the F_L band.
[b] S-A and S-B stand for *STEREO-A* and *STEREO-B*, respectively.
[c] STEREO-COR1 measurements during/close to the type II burst period.
[d] At the onset time of the type II burst (see column 4).
[e] Evolved into a "halo" CME in the *SOHO*-LASCO C2 FOV.
[f] S and G indicate Saito and Gopalswamy model, respectively. The prefixed numbers specify the density enhancement factor D.

Table 2
Shock Parameters Estimated from the Band-split of the Type II Bursts Listed in Table 1

S.No.	Date	Freq. Range (MHz)	$N_e(r)$ Model[a]	r_{typeII} ($R_\odot$)	BDW[b]	X[c]	M_A[d]	v_A[e] (km s^{-1})	$B(r)$[f] (G)
1	2013 Oct 08	68–51	2G	1.63–1.76	0.06	1.13	1.10	508–498	1.34–1.02
2	2013 Nov 08	60–37	2G	1.68–1.91	0.21	1.45	1.36	681–585	1.35–0.97
3	2013 Nov 19	61–36	17S	2.00–2.40	0.22	1.50	1.40	598–495	1.50–1.11
4	2014 Feb 10	43–38	9S	2.01–2.12	0.30	1.69	1.56	638–631	1.17–1.04

Notes.
[a] G and S indicate the Saito and Gopalswamy coronal electron density model, respectively. The prefixed numbers specify the density enhancement factor.
[b] Instantaneous bandwidth BDW $= (f_u - f_l)/f_l$, where f_l and f_u are the corresponding mid-frequencies in the F_L and F_U bands of the type II burst, respectively.
[c] Density jump across the shock $X = (\mathrm{BDW} + 1)^2$.
[d] Alfvénic Mach number $M_A = \sqrt{X(X+5)/2(4-X)}$.
[e] Alfvén speed $v_A = v_{cme}/M_A$.
[f] $B(r) = 5.1 \times 10^{-5} f_l v_A$.

above type II burst is ≈0.1 MHz s^{-1}. The density scale height in the 6× Saito model is ≈2.3×10^5 km. This is nearly the same as the typical density scale height for the coronal streamers at $r \gtrsim 1.5\,R_\odot$ (Aschwanden & Acton 2001). Considering that the CMEs are also density enhancements like the streamers, the similarity is possible. We also used the correspondence between the starting frequency (f) of the type II bursts and the distance (r) of the associated CME LE, i.e., $f(r) = 307.87 r^{-3.78} - 0.14$, to estimate v_{typeII} (Gopalswamy et al. 2013). Note that the above power-law relationship should be converted to a "model" (hereinafter referred to as the Gopalswamy model) for $N_e(r)$ to calculate v_{typeII}. We used the equality $f(r) = 9 \times 10^{-3}\sqrt{N_e(r)}$, where $f(r)$ and $N_e(r)$ are in units of MHz and cm^{-3}, respectively, for this purpose. The density was enhanced by a factor of two (i.e., 2× Gopalswamy model) to meet criteria 1 and 2 listed above for the CME-type II burst association in the case of the 2013 November 8 event. The estimated $v_{typeII} \approx 635$ km s^{-1} agrees closely with the aforementioned v_{CME}.

We calculated the associated coronal magnetic field strength ($B(r)$) from the split-band characteristics of the type II burst of 2013 November 8, following the methodology described in Vršnak et al. (2002), Cho et al. (2007). The results indicate that $B(r) \approx 1.8$–1.3 G in the range $r \approx 1.67$–$1.97\ R_\odot$ in the case of 6× Saito model. For 2× Gopalswamy model, $B(r) \approx$ 1.35–0.97 G in the range $r \approx 1.68$–$1.91\ R_\odot$. Note that the above distance ranges correspond to the frequency interval of 60-37 MHz over which both the F_L and F_U bands in the 2013 November 8 type II burst were observed with the GLOSS (see Figure 1). Based on similar CME-associated type II burst observations and independent electron density estimates, Zucca et al. (2014) recently reported $B \approx 1$ G at $r \approx 1.6\ R_\odot$. The corresponding plasma frequency was 70 MHz. These numbers

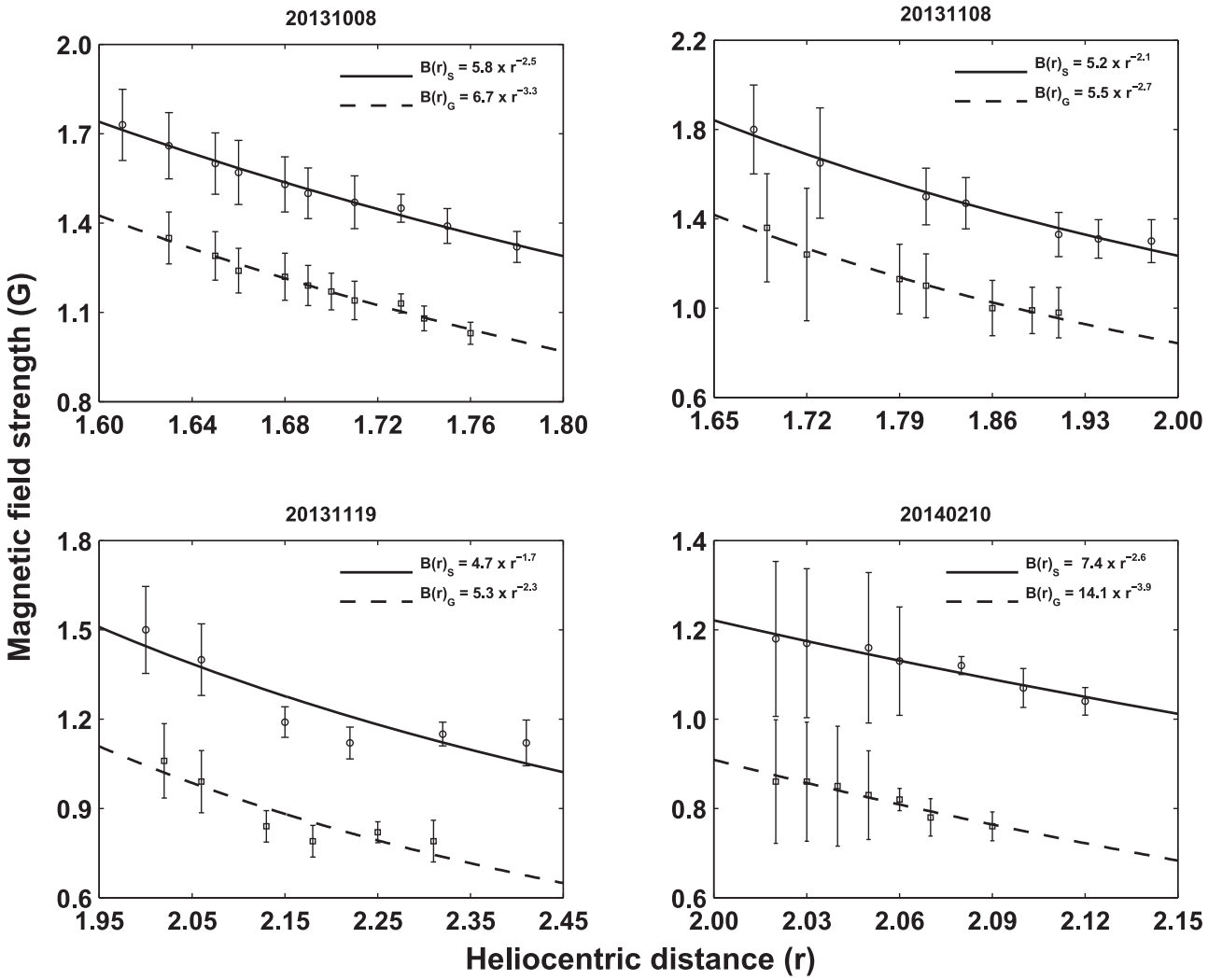

Figure 4. $B(r)$ estimates from the split-band type II bursts reported in the present work (see Table 1). The "circle" and "square" symbols correspond to the Saito (S) and Gopalswamy (G) models, respectively. The "solid" and "dashed" lines are the power-law fit to the estimates using the above two models. The error bars are due to the spectral width of the F_L and F_U bands.

are in good agreement with our above results. We carried out similar analysis for the other type II bursts reported in the present work, by using both the Saito and Gopalswamy models. The results are listed in columns 11–13 of Table 1. The associated shock parameters are listed in Table 2. The $r_{\rm typeII}$ (corresponding to the start frequency of the type II bursts in our observations) and $r_{\rm CME}$ (at the epoch corresponding to $r_{\rm typeII}$) agree closely for all the events in both the models. This indicates that we are using the appropriate distribution of $N_e(r)$ for each event. Note that the CME associated with one of the split-band type II bursts (2013 November 19) evolved into a "halo" CME in the *SOHO*-LASCO C2 FOV (see column 9 in Table 1). This probably could be the reason for the higher value of D in both the Saito and Gopalswamy models for the above event. We would like to add here that the D values used in the $N_e(r)$ model for each event (see column 10 of Table 1) are consistent with: (1) those reported earlier for radio observations associated with large-scale density enhancements like the CMEs and coronal streamers in the solar atmosphere (Sastry et al. 1981, 1983; Lantos et al. 1987; Schmahl et al. 1994; Ramesh et al. 2001; Kathiravan et al. 2002; Kathiravan & Ramesh 2004, 2005; Subramanian 2004); (2) recent observations by Morosan et al. (2014) which indicate that plasma levels corresponding to ≈60–30 MHz as in the present case (see column 3 in Table 1) can occur at heliocentric distances as large as $r \approx 2.5$–$4.0\ R_\odot$ when there is a CME. We found that for this to happen, the value of D as per the Saito model used in the present work should be $\gtrsim$35; (3) whitelight coronagraph observations of CME-associated MHD shock indicate that even the POS density ahead of the propagating CME front is enhanced by $\gtrsim$10× for "halo" CMEs at $r \approx 6\ R_\odot$ (Vourlidas et al. 2003; Ontiveros & Vourlidas 2009). This implies that the enhancement could be larger when the CMEs are located comparatively closer to the Sun, since the size of the CMEs increase as they propagate (Gopalswamy et al. 2012a). This probably could be the reason for the comparatively larger density enhancement factor for the event of 2013 November 19, in both the Saito and Gopalswamy models (see column 10 in Table 1).

Figure 4 shows the estimates of B from each split-band type II burst reported in the present work using $D\times$ Saito and $D\times$ Gopalswamy models. They are in the range of B values reported in the literature from some of the other CME-associated phenomena like moving type IV bursts and quasi-periodic type III bursts in the "middle" corona (Bastian et al. 2001; Ramesh et al. 2003a, 2003b; Sasikumar Raja

et al. 2014; Hariharan et al. 2016). A comparison with the non-flaring corona case indicates that the present estimates are ≈2× larger (Gopalswamy et al. 1986; Ramesh et al. 2011). Our interest is to obtain $B(r)$. Since the number of events is limited, we treated them separately and used an independent power-law fit of the type $B(r) = Cr^{-\alpha}$ for each of them (see Figure 4). An inspection of the $B(r)$ profiles indicates that they are different for the above two models. The B values estimated using the $D\times$ Saito model are ≈1.2 times larger in each event. Since $B \propto \sqrt{N_e}$, this is primarily due to the differences between the two density models and the use of comparatively larger values of D in the Saito model (see column 10 in Table 1) to satisfy the criteria mentioned earlier to select the coronal electron density model. Note that one of the main criteria used in the present work to constrain B is that $v_{\rm typeII}$ should be close to $v_{\rm CME}$ for each event. We note from columns 8 and 12 in Table 1 that for the 1st and 2nd events in the list, the above two quantities agree closely if we use the Gopalswamy model. The differences are ≈4 km s^{-1} (2013 October 8) and ≈84 km s^{-1} (2013 November 8). For the 3rd and 4th events, the use of the Saito model gives better agreement between $v_{\rm typeII}$ and $v_{\rm CME}$. The differences are ≈183 km s^{-1} (2013 November 19) and ≈53 km s^{-1} (2014 February 10). There is excellent agreement between $v_{\rm typeII}$ and $v_{\rm CME}$ (difference <100 km), except for the event of 2013 November 19, where the difference is comparatively higher (≈183 km s^{-1}). The latter could be due to possible uncertainties in identifying the CME LE and hence the estimate of $v_{\rm CME,}$ since the associated CME evolved into a "halo" event, as mentioned earlier. Having identified the most suitable coronal electron density model for each event, as mentioned above, we then compared the radial variation in the corresponding $B(r)$. It is steepest ($r^{-3.3}$) for the event of 2013 October 8, which was observed closest to the Sun in the range $r \approx 1.63$–$1.76\ R_\odot$. Following the above, are the events of 2013 November 8 with $r^{-2.7}$ in the range $r \approx 1.68$–$1.91\ R_\odot$, and 2014 February 10 with $r^{-2.6}$ in the range $r \approx 2.01$–$2.12\ R_\odot$. The variation is shallowest ($r^{-1.7}$) for the event of 2013 November 19, which was observed farthest from the Sun in the range $r \approx 2.00$–$2.40\ R_\odot$ (see columns 11 and 13 in Table 1, and Figure 4). Although the number of events in the present case are limited, we find that the above trend in the radial variation is consistent with the general scenario where the influence of the active region magnetic fields on B decreases with increasing distance from the Sun, and the $B(r)$ profile finally ends up with a nearly r^{-2} variation (see for example Pätzold et al. 1987; Poomvises et al. 2012). Note that the radial variation of B in all the above four cases is gradual compared to the typical r^{-6} variation of $N_e(r)$ in the "middle" corona. This implies that the corresponding Alfvén speed ($v_A(r)$) should exhibit a turn over, which is an important criterion in the shock formation and generation of type II bursts (see for example Gopalswamy et al. 2001).

4. SUMMARY

We estimated the solar coronal magnetic field strength from four CME-associated type II solar radio bursts that exhibited *F–H* emission and split-band characteristics. Upon imposing the constraint that the relevant coronal electron density distribution model should satisfy the observed parameters of the type II bursts and the associated CMEs together, our results suggest that the field strengths are unique to each type II burst. But a comparison of the radial variation of B in the different type II bursts indicates that they follow a pattern. The closer the heliocentric distance range of the type II burst to the Sun, the steeper is the variation. Since, currently, it is difficult to measure B in the "middle" corona at other spectral bands in the electromagnetic spectrum, it is hoped that more "radio" estimates of $B(r)$ with tight constraints, as in the present work, will be useful particularly for the shock acceleration theories.

We thank the staff of the Gauribidanur Observatory for their help with observations, and maintenance of the antenna and receiver systems there. We are grateful to the referee for his/her kind comments, which helped us to present the results more clearly. The *SOHO* data are produced by a consortium of the Naval Research Laboratory (USA), Max-Planck-Institut fuer Aeronomie (Germany), Laboratoire d'Astronomie (France), and the University of Birmingham (UK). *SOHO* is a project of international cooperation between ESA and NASA. The *SOHO*-LASCO CME catalog and STEREO movies are generated and maintained at the CDAW Data Center by NASA and the Catholic University of America in cooperation with the Naval Research Laboratory. NG was supported by NASA's LWS TR&T program.

REFERENCES

Allen, C. W. 1947, MNRAS, 107, 426
Aschwanden, M. J., & Acton, L. W. 2001, ApJ, 550, 475
Bastian, T. S., Pick, M., Kerdraon, A., Maia, D., & Vourlidas, A. 2001, ApJL, 558, L65
Baumbach, S. 1937, AN, 263, 120
Benz, A. O., Monstein, Ch., Meyer, H., et al. 2009, EM&P, 104, 277
Brueckner, G. E., Howard, R. A., Koomen, M. J., et al. 1995, SoPh, 162, 357
Cho, K.-S., Bong, S.-C., Kim, Y.-H., et al. 2008, A&A, 491, 873
Cho, K.-S., Gopalswamy, N., Kwon, R.-Y., Kim, R.-S., & Yashiro, S. 2013, ApJ, 765, 148
Cho, K.-S., Lee, J., Gary, D. E., Moon, Y.-J., & Park, Y. D. 2007, ApJ, 665, 799
Ebenezer, E., Ramesh, R., Subramanian, K. R., Sundara Rajan, M. S., & Sastry, Ch. V. 2001, A&A, 367, 1112
Ebenezer, E., Subramanian, K. R., Ramesh, R., Sundara Rajan, M. S., & Kathiravan, C. 2007, BASI, 35, 111
Gopalswamy, N., Aguilar-Rodriguez, E., Yashiro, S., Nunes, S., & Kaiser, M. L. 2005, JGR, 110, A12S07
Gopalswamy, N., & Kundu, M. R. 1992, in AIP Conf. Proc. 264, Particle Acceleration in Cosmic Plasmas, ed. G. P. Gaisser & T. K. Zank (Melville, NY: AIP), 257
Gopalswamy, N., Lara, A., Kaiser, M. L., & Bougeret, J.-L. 2001, JGR, 106, 25261
Gopalswamy, N., Mäkelä, P., Yashiro, S., & Davila, J. M. 2012a, SunGe, 7, 7
Gopalswamy, N., Nitta, N., Akiyama, S., Mäkelä, P., & Yashiro, S. 2012b, ApJ, 744, 72
Gopalswamy, N., Thejappa, G., Sastry, Ch. V., & Tlamicha, A. 1986, BAICz, 37, 115
Gopalswamy, N., Thompson, B. J., Davila, J. M., et al. 2009, SoPh, 259, 227
Gopalswamy, N., Xie, H., Mäkelä, P., et al. 2013, AdSpR, 51, 1981
Hariharan, K., Ramesh, R., & Kathiravan, C. 2015, SoPh, 290, 2479
Hariharan, K., Ramesh, R., Kathiravan, C., & Wang, T. J. 2016, SoPh, 291, 1405
Hariharan, K., Ramesh, R., Kishore, P., Kathiravan, C., & Gopalswamy, N. 2014, ApJ, 795, 14
Howard, R. A., Moses, J. D., Vourlidas, A., et al. 2008, SSRv, 136, 67
Kathiravan, C., & Ramesh, R. 2004, ApJ, 610, 532
Kathiravan, C., & Ramesh, R. 2005, ApJL, 627, L77
Kathiravan, C., Ramesh, R., & Subramanian, K. R. 2002, ApJL, 567, L93
Kishore, P., Kathiravan, C., Ramesh, R., Indrajit, V., & Barve Rajalingam, M. 2014, SoPh, 289, 3995
Kishore, P., Ramesh, R., Kathiravan, C., & Rajalingam, M. 2015, SoPh, 290, 2409
Kouloumvakos, A., Patsourakos, S., Hillaris, A., et al. 2014, SoPh, 289, 2123
Lantos, P., Alissandrakis, C. E., Gergely, T., & Kundu, M. R. 1987, SoPh, 112, 325
Leblanc, Y., Dulk, G. A., & Bougeret, J.-L. 1998, SoPh, 183, 165

Lee, J. 2007, SSRv, 133, 73
Lin, H., Penn, M. J., & Tomczyk, S. 2000, ApJL, 541, L83
Lin, J., Mancuso, S., & Vourlidas, A. 2006, ApJ, 649, 1110
Liu, Y., Luhmann, J. G., Bale, S. D., & Lin, R. P. 2009, ApJL, 691, L151
Ma, S., Raymond, J. C., Golub, L., et al. 2011, ApJ, 738, 160
Mancuso, S., & Garzelli, M. V. 2013, A&A, 553, A100
Mancuso, S., & Raymond, J. C. 2004, A&A, 413, 363
Mann, G., Klassen, A., Classen, H.-T., et al. 1996, A&AS, 119, 489
Monstein, C., Ramesh, R., & Kathiravan, C. 2007, BASI, 35, 473
Morosan, D. E., Gallagher, P. T., Zucca, P., et al. 2014, A&A, 568, A67
Nelson, G. J., & Melrose, N. R. 1985, in Solar Radio Physics, ed. D. J. McLean & N. R. Labrum (Cambridge: Cambridge Univ. Press), 333
Newkirk, G., Jr 1961, ApJ, 133, 983
Ontiveros, V., & Vourlidas, A. 2009, ApJ, 693, 267
Pätzold, M., Bird, M. K., Volland, H., et al. 1987, SoPh, 109, 91
Poomvises, W., Gopalswamy, N., Yashiro, S., Kwon, R.-Y., & Olmedao, O. 2012, ApJ, 758, 118
Ramesh, R. 2011, in Proc. 1st Asia-Pacific Solar Physics Meeting, ASInC, ed. A. R. Choudhuri & D. Banerjee (Bangalore: ASI), 55
Ramesh, R., Anna Lakshmi, M., Kathiravan, C., Gopalswamy, N., & Umapathy, S. 2012, ApJ, 752, 107
Ramesh, R., Kathiravan, C., & Sastry, Ch. V. 2001, ApJL, 548, L229
Ramesh, R., Kathiravan, C., & Sastry, Ch. V. 2003a, ApJL, 591, L163
Ramesh, R., Kathiravan, C., & Satya Narayanan, A. 2011, ApJ, 734, 39
Ramesh, R., Kathiravan, C., Satya Narayanan, A., & Ebenezer, E. 2003b, A&A, 400, 753
Ramesh, R., Kathiravan, C., Sreeja, S. K., & Gopalswamy, N. 2010, ApJ, 712, 188
Ramesh, R., Kishore, P., Sargam, M., et al. 2013, ApJ, 778, 30
Ramesh, R., Subramanian, K. R., Sundara Rajan, M. S., & Sastry, Ch. V. 1998, SoPh, 181, 439
Saito, K., Poland, A. I., & Munro, R. H. 1977, SoPh, 55, 121
Sasikumar Raja, K., Ramesh, R., Hariharan, K., Kathiravan, C., & Wang, T. J. 2014, ApJ, 796, 56
Sastry, Ch. V., Dwarakanath, K. S., Shevgaonkar, R. K., & Krishan, V. 1981, SoPh, 73, 363
Sastry, Ch. V., Shevgaonkar, R. K., & Ramanuja, M. N. 1983, SoPh, 87, 391
Schatten, K. H., Wilcox, J. M., & Norman, F. 1969, SoPh, 6, 442
Schmahl, E. J., Gopalswamy, N., & Kundu, M. R. 1994, SoPh, 150, 325
Schrijver, C. J., & Derosa, M. L. 2003, SoPh, 212, 165
Smerd, S. F., Sheridan, K. V., & Stewart, R. T. 1974, in IAU Symp. 57, Coronal Disturbances, ed. G. A. Newkirk (Dordrecht: Reidel), 389
Smerd, S. F., Sheridan, K. V., & Stewart, R. T. 1975, ApL, 16, 23
Stewart, R. T., Howard, R. A., Hansen, F., Gergely, T., & Kundu, M. R. 1974a, SoPh, 36, 219
Stewart, R. T., McCabe, M. K., Koomen, M. J., Hansen, R. T., & Dulk, G. A. 1974b, SoPh, 36, 203
Subramanian, K. R. 2004, A&A, 426, 329
Tidman, D. A., Birmingham, T. J., & Stainer, H. M. 1966, ApJ, 146, 207
Vasant, V., Umapathy, S., Vršnak, B., Žic, T., & Prakash, O. 2014, SoPh, 289, 251
Vourlidas, A., Wu, S. T., Wang, A. H., Subramanian, P., & Howard, R. A. 2003, ApJ, 598, 1392
Vršnak, B., Aurass, H., Magdalenić, J., & Gopalswamy, N. 2001, A&A, 377, 321
Vršnak, B., Magdalenić, J., Aurass, H., & Mann, G. 2002, A&A, 396, 673
Vršnak, B., Magdalenić, J., & Zlobec, P. 2004, A&A, 413, 753
West, M. J., Zhukov, A. N., Dolla, L., & Rodriguez, L. 2011, ApJ, 730, 122
Zimovets, I., Vilmer, N., Chian, A. C.-L., Sharykin, I., & Struminsky, A. 2012, A&A, 547, A6
Zucca, P., Carley, E. P., Bloomfield, D. S., & Gallagher, P. T. 2014, A&A, 564, A47